ORIGINAL ARTICLE

lajss.org© Latin American Journal of Solids and Structures

www.lajss.org

Structural behavior and failure modes of steel- and GFRP-reinforced geopolymer concrete slabs strengthened with FRCM: experimental and numerical study

Thuy Chi Dang[a], Huy Cuong Nguyen[a*], Cong Hau Nguyen[a]

[a] University of Transport and Communications, No. 3 Cau Giay Street, Lang Ward, Hanoi, Vietnam. Email: thuychi.dang@utc.edu.vn, nguyenhuycuong@utc.edu.vn, haunc_ph@utc.edu.vn

* Corresponding author

https://doi.org/10.1590/1679-7825/e9019

Abstract

This study presents an experimental–numerical investigation on one-way geopolymer concrete (GPC) slab strips internally reinforced with steel or GFRP bars and externally strengthened using a glass fabric-reinforced cementitious matrix (FRCM) system. Six full-scale specimens were tested under four-point bending to characterize cracking response, stiffness evolution, strengthening efficiency, and governing failure mechanisms. The steel-reinforced control slab exhibited a ductile flexure-controlled failure. With glass-FRCM strengthening, the ultimate load increased by approximately 31% for one layer and 59% for two layers, accompanied by improved crack distribution and enhanced post-cracking stiffness, while maintaining flexural dominance. In contrast, the GFRP-reinforced control slab failed in shear, highlighting the limited stress redistribution associated with the lower elastic modulus and linear-elastic behavior of GFRP bars. Glass-FRCM strengthening improved tensile stiffness and crack control; however, the strengthened GFRP slabs remained shear-governed, indicating that flexural strengthening alone may be insufficient to prevent premature diagonal cracking. Overall, the results demonstrate that strengthening effectiveness is strongly dependent on the internal reinforcement type, and that additional shear strengthening measures are required for GFRP-reinforced GPC slab systems.

Keywords

Geopolymer concrete, GFRP reinforcement, Steel reinforcement, Fabric-reinforced cementitious matrix (FRCM), Flexural behavior, Shear failure

Received February 23, 2026. In revised form March 19, 2026. Accepted March 19, 2026. Available online March 23, 2026.
https://doi.org/10.1590/1679-7825/e9019

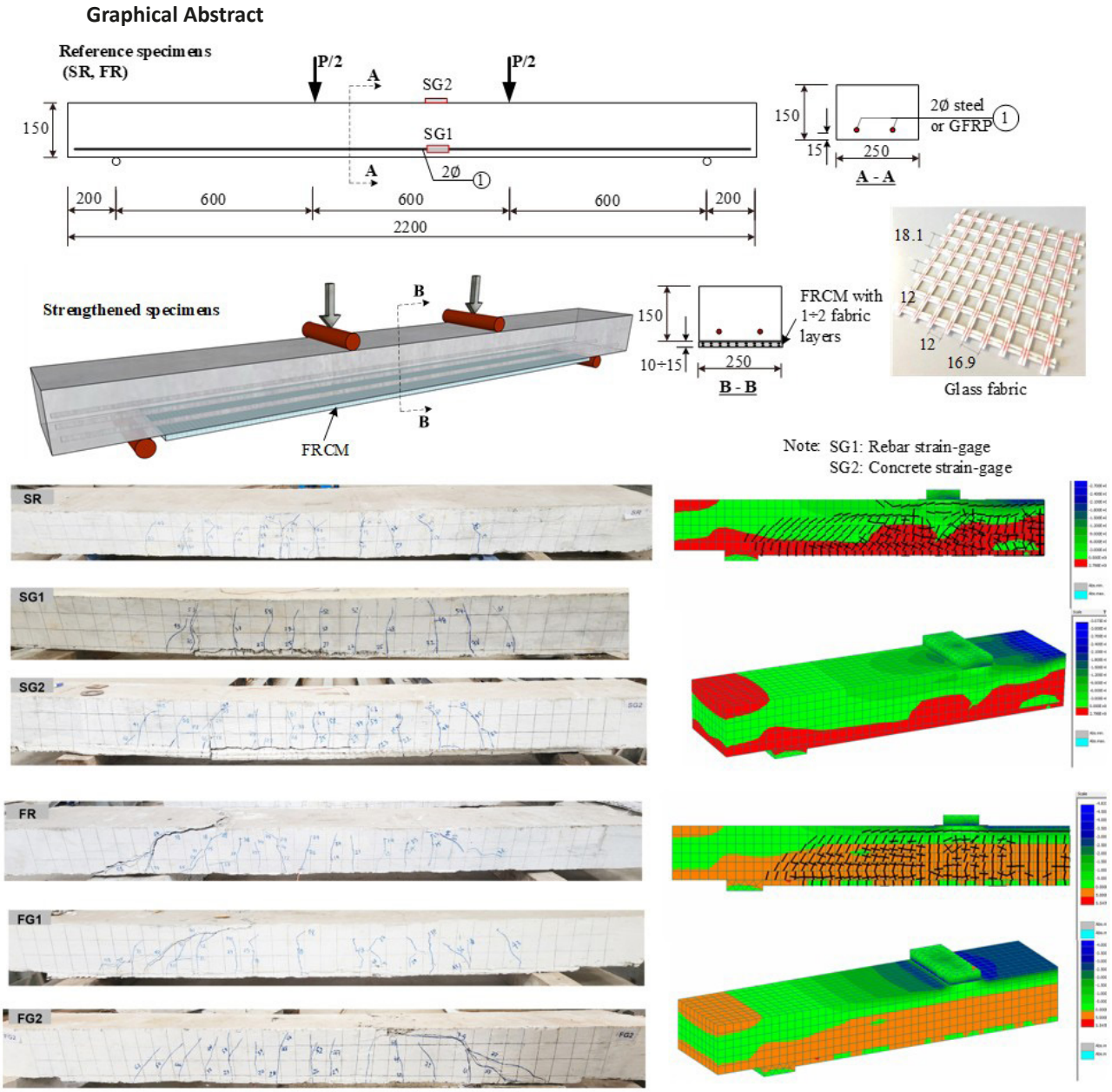

1 INTRODUCTION

The growing demand for sustainable construction materials has intensified research into geopolymer concrete (GPC) as an alternative to ordinary Portland cement (OPC). By utilizing industrial by-products such as fly ash and ground granulated blast furnace slag, geopolymer binders significantly reduce CO_2 emissions while maintaining competitive mechanical performance. Azunna et al. (2022) reported that reinforced geopolymer concrete elements demonstrate structural behavior comparable to conventional concrete, while emphasizing the need for further investigation into serviceability and composite interaction mechanisms.

Recent experimental investigations confirm that GPC beams exhibit adequate compressive strength, flexural capacity, and bond characteristics. Udhaya Kumar et al. (2020) demonstrated that geopolymer aggregate concrete beams achieved satisfactory bond strength and flexural performance under monotonic loading, confirming the viability of GPC for structural applications.

Parallel to binder innovation, the replacement of steel reinforcement with fiber-reinforced polymer (FRP) bars—particularly glass FRP (GFRP)—has gained attention due to corrosion resistance and high tensile strength. Maranan et al. (2015) reported that GFRP-reinforced geopolymer concrete beams achieved satisfactory flexural strength but exhibited larger deflections and wider cracks because of the lower elastic modulus of GFRP. Hasan et al. (2021) further confirmed that GFRP-reinforced geopolymer T-beams demonstrate flexure-controlled behavior while remaining sensitive to

reinforcement stiffness and bond characteristics. Numerical investigations by George et al. (2022) and Kadhim and Zinkaah (2023) reinforced these findings, indicating that hybrid or GFRP reinforcement alters stiffness distribution and may influence failure mode transitions. Despite these advances, current design provisions remain largely adapted from steel-reinforced concrete and do not fully address the combined behavior of geopolymer matrices and FRP reinforcement.

Strengthening strategies are equally critical, particularly for aging infrastructure or members deficient in flexure or shear. While externally bonded FRP systems are widely used, their reliance on epoxy matrices limits high-temperature performance and compatibility with concrete substrates. Fabric-reinforced cementitious matrix (FRCM) systems, also referred to as TRM or TRC, overcome these drawbacks through the use of inorganic matrices. D'Ambrisi and Focacci (2011) experimentally confirmed that FRCM systems provide effective flexural strengthening while exhibiting distinct debonding mechanisms governed by fiber–matrix interaction. Schladitz et al. (2012) demonstrated substantial load-bearing capacity enhancement and reduced deflection in reinforced concrete slabs strengthened with textile-reinforced concrete.

Recent studies extended these concepts to geopolymer-based matrices. Zhang et al. (2021) reported significant flexural capacity enhancement in concrete slabs strengthened with textile-reinforced geopolymer mortar, highlighting improved crack control and composite action. Alexander and Shashikala (2022) further demonstrated that carbon textile-reinforced geopolymer mortar improved flexural strength by up to 80% in rehabilitated beams, confirming the potential synergy between geopolymer matrices and textile systems. However, most existing investigations focus either on steel-reinforced OPC concrete strengthened with FRCM (D'Ambrisi and Focacci, 2011; Schladitz et al., 2012) or on geopolymer concrete reinforced with GFRP bars without cementitious textile strengthening (Hasan et al., 2021; Maranan et al., 2015). Although Junaid et al. (2020) examined GFRP-reinforced geopolymer beams strengthened with externally bonded composites, the interaction between low-modulus internal reinforcement and cementitious textile systems remains insufficiently clarified, particularly with respect to flexural–shear failure transition.

In shear applications, FRCM systems have also shown promising performance. Elsamak et al. (2020) demonstrated that fully wrapped FRCM jackets can increase shear capacity by up to 70%, while Soliman et al. (2023) highlighted the critical role of fabric configuration and matrix properties in predicting shear contribution. Nevertheless, reliable predictive models remain limited, and the interaction between internal FRP reinforcement and external FRCM systems is insufficiently understood.

Despite the growing body of research, a clear knowledge gap persists regarding the integrated structural behavior of geopolymer concrete slabs internally reinforced with GFRP bars and externally strengthened using FRCM systems. The combined influence of low-modulus GFRP reinforcement and cementitious textile strengthening on stiffness evolution, cracking response, and failure mode has not been systematically examined. Existing design frameworks do not provide explicit guidance for such hybrid systems, particularly concerning the transition between flexural- and shear-dominated mechanisms.

To the authors' knowledge, no previous study has experimentally compared steel- and GFRP-reinforced GPC slabs strengthened with FRCM under identical geometric and loading conditions. Accordingly, the present study experimentally and numerically investigates six full-scale geopolymer concrete slab strips internally reinforced with steel or GFRP bars and externally strengthened using glass FRCM. The objectives are: (i) to quantify the influence of reinforcement type on load–deflection behavior and failure mode; (ii) to evaluate the strengthening efficiency of one- and two-layer FRCM systems; and (iii) to clarify the governing mechanisms controlling flexural–shear response in hybrid geopolymer–FRP–FRCM members.

The research contributes to advancing sustainable structural systems by integrating low-carbon geopolymer binders with corrosion-resistant reinforcement and inorganic composite strengthening. The findings provide experimental evidence and validated numerical modeling results that support the development of more reliable design approaches for next-generation resilient concrete structures.

2 EXPERIMENTAL PROGRAM

2.1 Specimen design and reinforcement configuration

The experimental program comprised six full-scale GPC slab strips designed to investigate the combined influence of internal reinforcement type and external FRCM strengthening on flexural behavior. All specimens had identical geometry, with a total length of 2200 mm, a clear span of 1800 mm, and a rectangular cross-section of 250 mm × 150 mm (Figure 1). The four-point bending configuration generated a constant moment region between the loading points and equal shear spans of 600 mm, resulting in a shear span-to-effective depth ratio (a/d) of approximately 4.65, which lies within the flexure-dominated range.

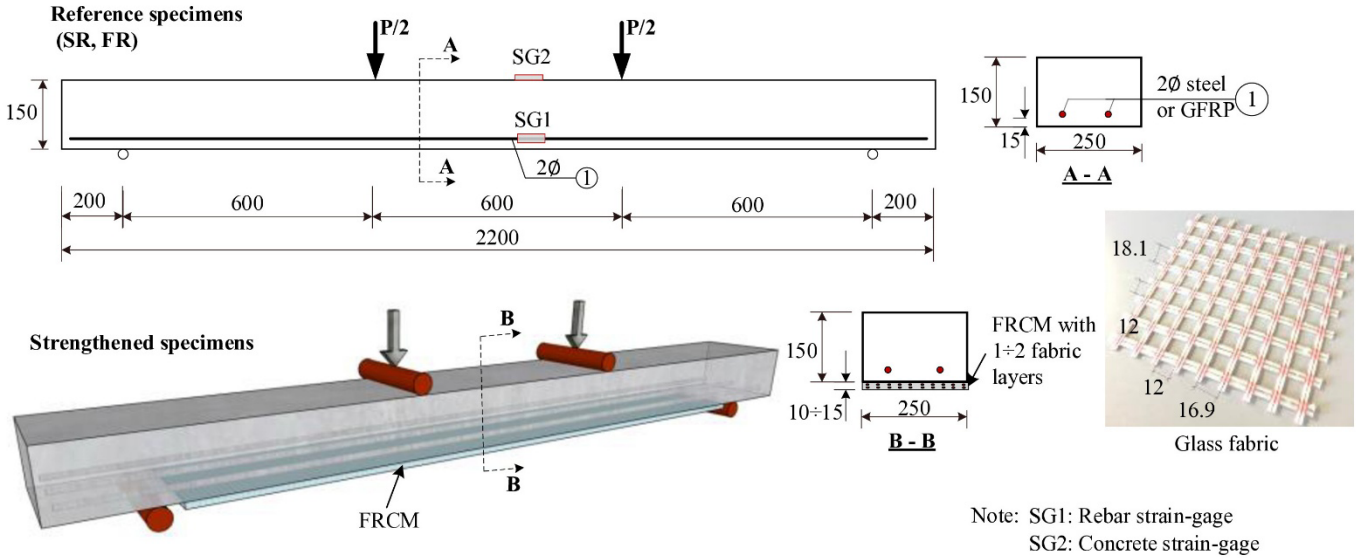

Figure 1: Geometry and reinforcement layout of tested slabs

To replicate the behavior of one-way slab strips, no transverse shear reinforcement was provided. This detailing reflects common slab practice, where shear resistance is primarily carried by the concrete section. Two longitudinal bars were placed in the tension zone of each slab. Steel-reinforced specimens were provided with two deformed D12 bars, while GFRP-reinforced specimens contained two straight D12 GFRP bars with equivalent tensile reinforcement area. Adequate development length was ensured for both reinforcement types, and a concrete cover of 15 mm was maintained.

Two specimens were tested without external strengthening and served as control members, namely SR (steel-reinforced) and FR (GFRP-reinforced). The remaining specimens were externally strengthened using one or two layers of glass fabric-reinforced cementitious matrix (FRCM), designated as SG1 and SG2 for the steel-reinforced slabs and FG1 and FG2 for the GFRP-reinforced slabs. The FRCM layers were bonded to the soffit and consisted of bidirectional alkali-resistant glass fabric embedded within approximately 5 mm thick layers of fine-grained mortar. The strengthening system was applied continuously along the full span to promote uniform stress transfer and effective composite action. It should be noted that each strengthening configuration was represented by a single specimen; therefore, the experimental matrix was primarily intended to identify comparative behavioural trends rather than to provide statistically robust validation.

To avoid premature local crushing at supports and loading points, 5 mm thick steel bearing plates were installed in these regions. The test matrix enabled a direct comparison between steel- and GFRP-reinforced GPC slabs and allowed assessment of the contribution of one and two FRCM layers under identical geometric and loading conditions, thereby isolating the governing flexural and shear mechanisms of the hybrid system.

2.2 Material properties

The GPC used for all specimens was produced from a binary binder system composed of Class F fly ash and ground granulated blast furnace slag, activated by a single-component dry alkaline powder. Natural river sand and crushed granite with a nominal size of 10–20 mm were used as fine and coarse aggregates, respectively. Sea sand was intentionally avoided to eliminate potential chloride-related durability concerns.

At 28 days, the GPC achieved an average compressive strength of 52.1 MPa. The measured flexural tensile strength and splitting tensile strength were 4.6 MPa and 3.77 MPa, respectively. The elastic modulus was approximately 28.4 GPa. These mechanical properties are consistent with structural-grade concrete suitable for flexural members under service and ultimate loading conditions.

The steel reinforcement exhibited a tensile strength of 439.6 MPa and a modulus of elasticity of 200 GPa. The GFRP bars had a tensile strength of 810 MPa and an elastic modulus of 45 GPa. Pull-out tests conducted between GFRP bars and GPC demonstrated stable bond–slip behavior, with an average peak bond stress of 16.74 MPa and corresponding slip values ranging from 1.04 mm to 1.57 mm. These results confirm adequate interfacial bond performance for structural applications.

The externally bonded FRCM strengthening system employed a bidirectional alkali-resistant glass fabric with a grid spacing of 17.5 mm and a surface weight of 647 g/m^2 (Figure 1). The yarns had a fineness of 2400 tex and were impregnated with styrene-butadiene rubber (SBR) to improve handling and bonding performance. The effective reinforcement area of the fabric was 105.67 mm^2/m in each principal direction. The glass fabric exhibited a tensile strength of 1580 MPa and a modulus of elasticity of 105 GPa. The cementitious matrix used to embed the glass fabric consisted of Portland cement,

fly ash, and quartz sand with a maximum particle size of 0.6 mm. The matrix achieved a compressive strength of 64.2 MPa and a flexural strength of 6.8 MPa.

2.3 Test setup and instrumentation

The experimental program was conducted in four main stages: (1) specimen fabrication and instrumentation, (2) surface preparation and application of the externally bonded FRCM overlay, (3) curing, and (4) structural testing under four-point bending. All slabs were cast in a single batch using a pan mixer to ensure uniform material properties and minimize variability. Before casting, steel or GFRP longitudinal reinforcement bars were instrumented with electrical resistance strain gauges positioned at midspan of the span length (Figure 2). An additional strain gauge was embedded at the top concrete surface at midspan to monitor compressive strain development.

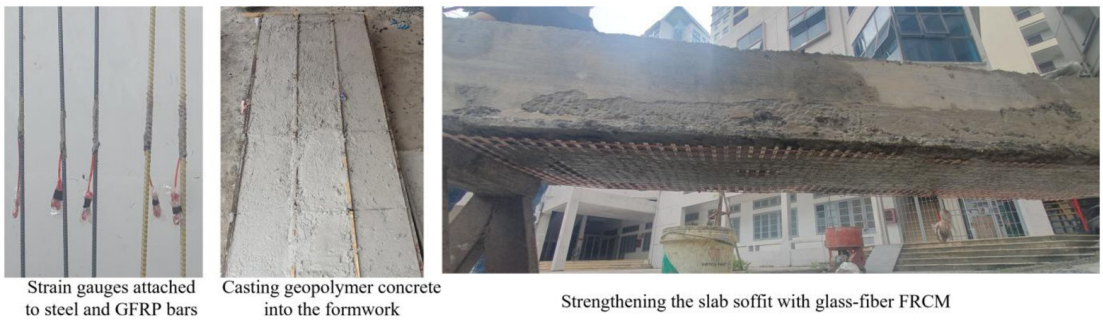

Figure 2: Preparation and strengthening procedures of geopolymer concrete

The externally bonded FRCM strengthening was installed in accordance with ACI Committee 549 (2020), ACI 549.4R-20, which provides design and construction guidelines for externally bonded FRCM systems. Prior to application, the soffit surface was mechanically roughened and cleaned to remove laitance and ensure adequate bond. The slab specimens were then positioned on a steel reaction frame to replicate field strengthening conditions (Figure 2). The FRCM overlay was applied from bottom to top, simulating overhead installation as typically performed in practical retrofitting works. A thin layer of cementitious matrix was first spread onto the prepared surface, followed by placement of the glass fabric, which was carefully pressed into the fresh matrix to ensure proper impregnation. A second mortar layer was subsequently applied to fully embed the fabric and achieve the target thickness. The system was cured under laboratory conditions to allow proper matrix hydration and bond development before structural testing.

After 28 days of curing, the specimens were tested under four-point bending using a 3000 kN SANS servo-hydraulic testing machine (Figure 3). The load was applied through a steel spreader beam, generating two symmetrically spaced point loads with a clear distance of 600 mm between the loading points. Loading was applied monotonically under displacement control at a rate of 1 mm/min until failure.

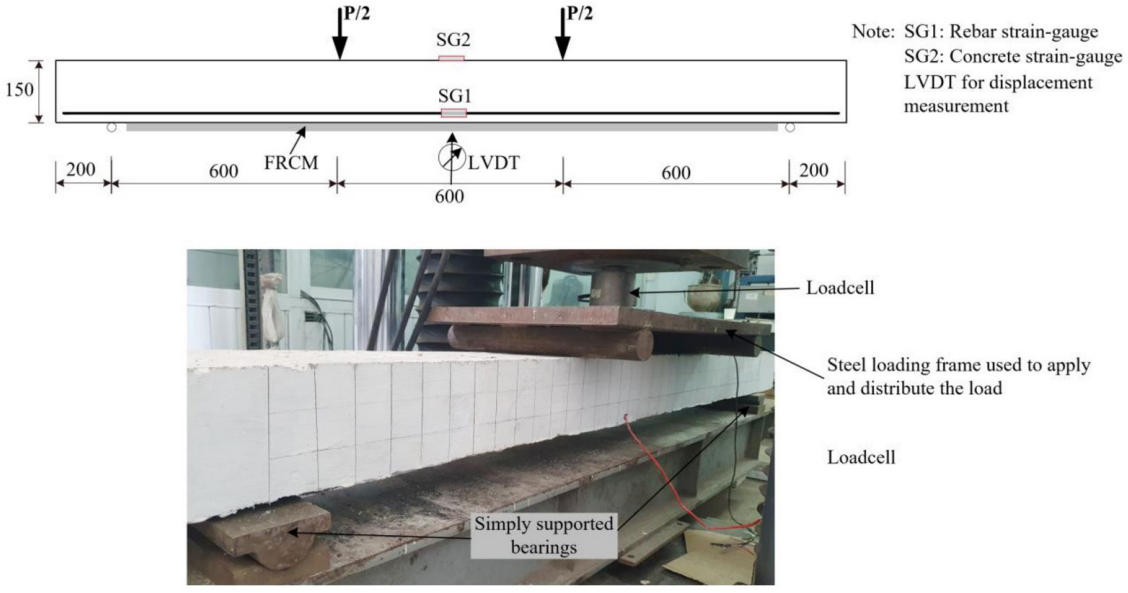

Figure 3: Test setup and loading configuration

Vertical deflection was measured using a linear variable differential transformer (LVDT) positioned at midspan. Strain data from the concrete surface and internal reinforcement were continuously recorded using a computerized data acquisition system. Crack initiation and propagation were monitored visually throughout the test using crack-width gauges. Crack patterns were mapped at different load levels. For FRCM-strengthened specimens, particular attention was given to potential failure mechanisms involving rupture of the glass fabric, cracking of the cementitious matrix, or debonding at the FRCM–concrete interface.

3 RESULTS AND DISCUSSION

3.1 Behavior of Steel-Reinforced GPC Slabs

3.1.1 Structural response of control slabs

The control specimen SR, reinforced with two D12 steel bars and without external FRCM strengthening, exhibited a typical flexure-dominated response characteristic of conventionally reinforced concrete slab strips. As shown in Figure 4-a, the load–deflection curve shows three distinct stages. In the initial uncracked stage, the response is nearly linear, indicating elastic behavior of both concrete and steel. The initial flexural stiffness is relatively high, and the midspan deflection increases proportionally with the applied load. First flexural cracking occurred at approximately 10 kN, corresponding to a visible reduction in stiffness. Beyond this point, the slope of the load–deflection curve decreased due to the loss of tensile capacity of the concrete in the cracked zone. The tensile force was progressively transferred to the steel reinforcement, as confirmed by the load–strain response. The steel tensile strain increased steadily after cracking, while the compressive strain at the top concrete fiber remained moderate.

The ultimate load of specimen SR reached approximately 42.4 kN. At higher load levels, the steel reinforcement approached yielding, as evidenced by a pronounced increase in tensile strain with limited additional load increment. The tensile strain in the steel reached approximately 8‰ at peak load, clearly indicating full mobilization of the reinforcement. In contrast, the compressive strain in concrete approached but did not exceed approximately 3‰, suggesting that failure was governed primarily by steel yielding rather than crushing of the compression zone. The post-peak behavior was characterized by increasing deflection with no significant load gain, reflecting a ductile flexural failure mechanism.

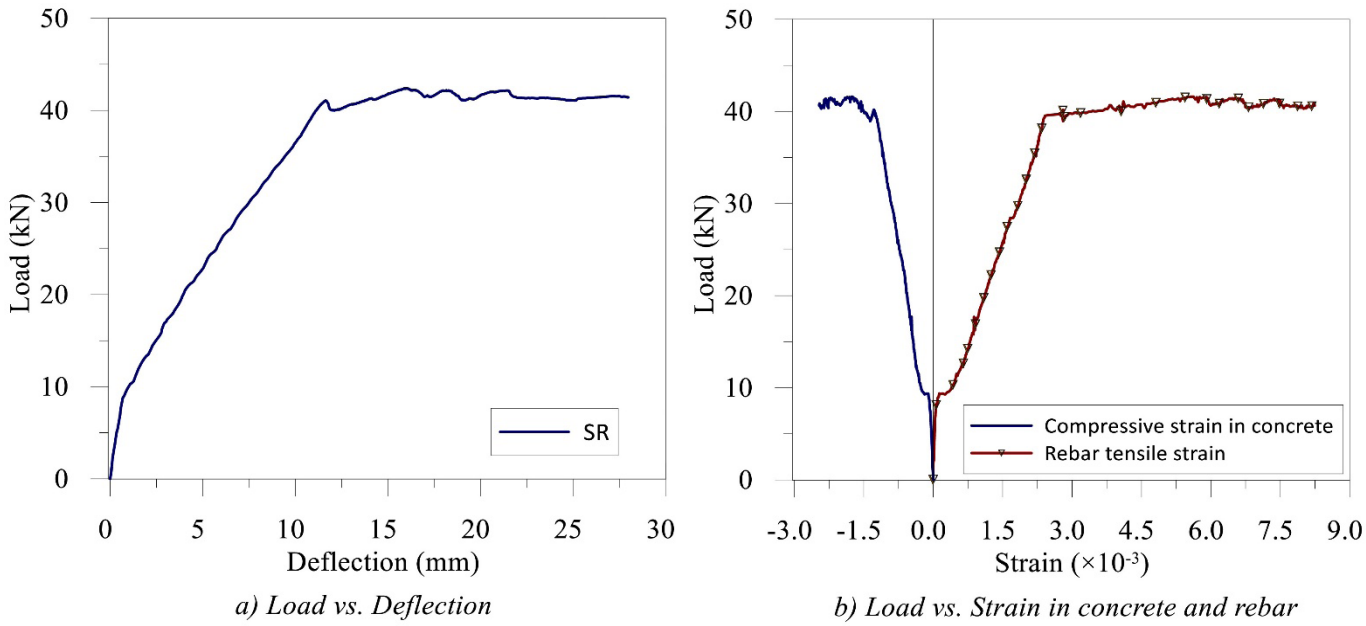

a) Load vs. Deflection *b) Load vs. Strain in concrete and rebar*

Figure 4: Load–deflection response (left) and strain development in concrete and tensile reinforcement (right) for specimen SR.

The crack pattern in Figure 5 further confirms bending-controlled behavior. Vertical flexural cracks initiated in the constant moment region and propagated upward toward the compression zone. Crack spacing was relatively uniform, and no diagonal shear cracks were observed within the shear spans. The absence of localized crack concentration or premature cover separation indicates stable stress redistribution after cracking.

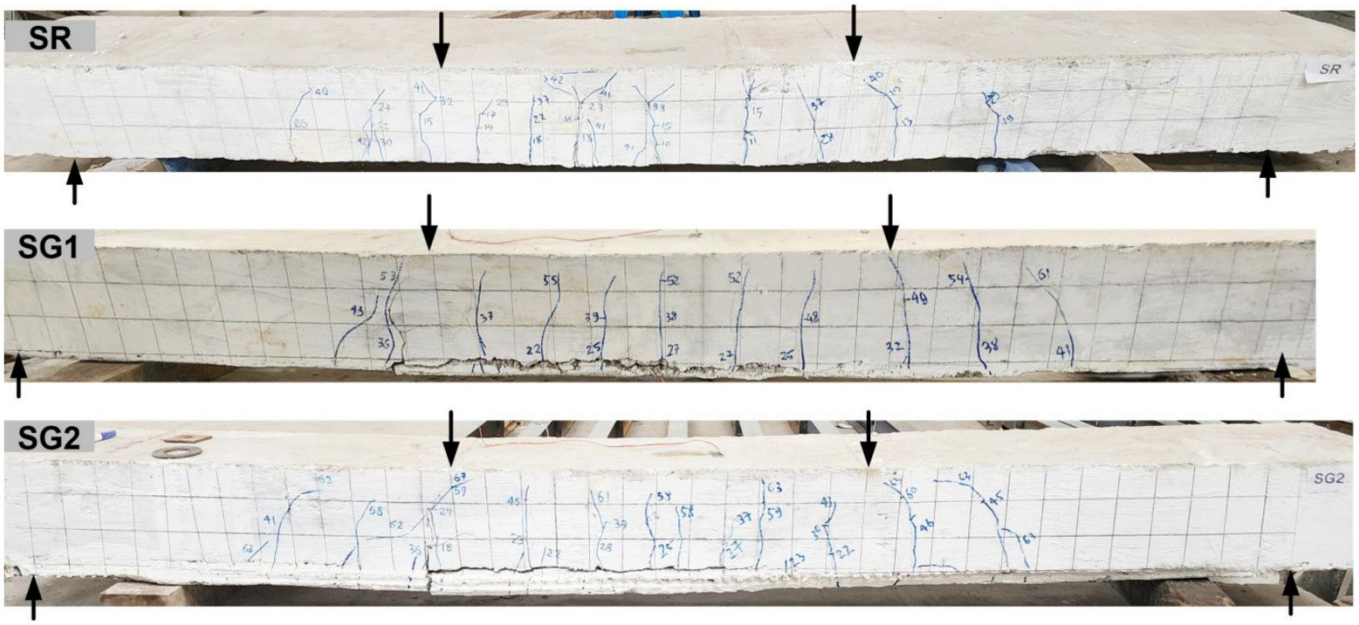

Figure 5: Crack patterns of control and FRCM-strengthened steel-reinforced slabs

3.1.2 Strengthening response of FRCM-retrofitted slabs

The responses of the steel-reinforced slabs (SR, SG1, and SG2) consistently indicate a flexure-governed mechanism, while clearly quantifying the role of the externally bonded FRCM in enhancing post-cracking stiffness, delaying yielding, and increasing the ultimate load. Figure 6 indicates that the FRCM-strengthened specimens exhibit only a marginal increase in global stiffness. This limited stiffness enhancement can be attributed to the relatively large shear span-to-depth ratio (a/d), under which flexural deformation dominates and the contribution of the externally bonded layer to pre-cracking stiffness remains minor. All three specimens display a nearly identical initial slope, confirming that the uncracked stiffness is primarily governed by the geopolymer concrete section and the internal steel reinforcement.

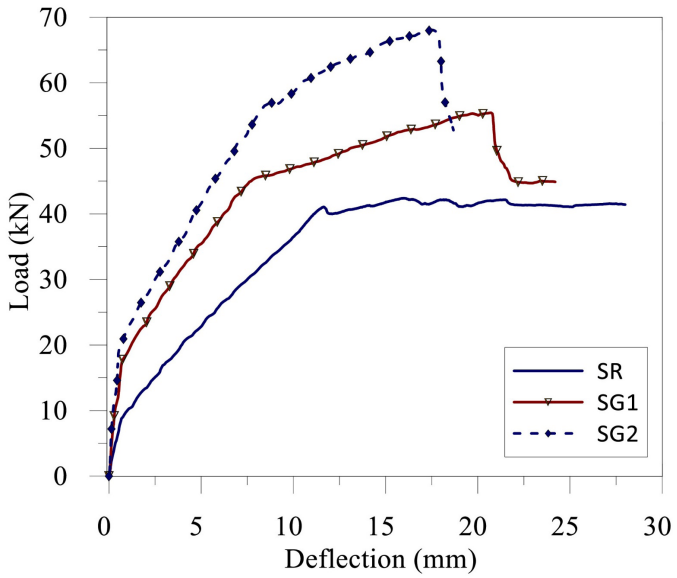

Figure 6: Load–deflection response of control and FRCM-strengthened slabs.

Nevertheless, a pronounced increase in cracking load was observed in the strengthened slabs, ranging from approximately 53% to 105%. This improvement is mainly associated with the high flexural tensile strength of the fine-grained mortar matrix and the effective bond between the glass fabric and the substrate, which enables early activation of the composite layer. The FRCM overlay contributes significantly after flexural cracking, when tensile stresses can no longer be sustained by the concrete and are progressively transferred to the steel reinforcement and the external

composite layer. This stress redistribution mechanism enhances crack control and delays stiffness degradation, leading to improved post-cracking performance.

Table 1: Summary of experimental results and governing failure modes

Specimen	Internal reinforcement	FRCM layers	Ultimate load (kN)	Increase vs control (%)	Governing failure mode
SR	Steel D12	0	42.4	-	Flexural (steel yielding)
SG1	Steel D12	1	55.7	31.3	Flexural failure (textile rupture)
SG2	Steel D12	2	67.6	59.4	
FR	GFRP D12	0	49.5	-	
FG1	GFRP D12	1	56.3	13.7	Shear-dominated
FG2	GFRP D12	2	60.9	23.1	

For the control slab SR, the peak load reached approximately 42.4 kN, after which the curve exhibits a pronounced plateau: the load stabilizes while deflection continues to increase. This response is typical of a conventional RC member whose post-cracking behavior is dominated by steel yielding and progressive crack opening. In contrast, the strengthened slabs reached markedly higher peak loads, namely 55.7 kN for SG1 (+31%) and 67.6 kN for SG2 (+59%), as shown in Table 1. Beyond strength enhancement, the strengthened specimens also developed a visibly steeper post-cracking slope, demonstrating that the FRCM layer contributes to tensile force sharing and partially restores stiffness after cracking. Importantly, the incremental benefit from one to two fabric layers is evident not only in ultimate load but also in the sustained stiffness at intermediate deflection levels: at comparable midspan deflections, SG2 consistently carries higher loads than SG1, confirming the effective mobilization of the additional fabric layer.

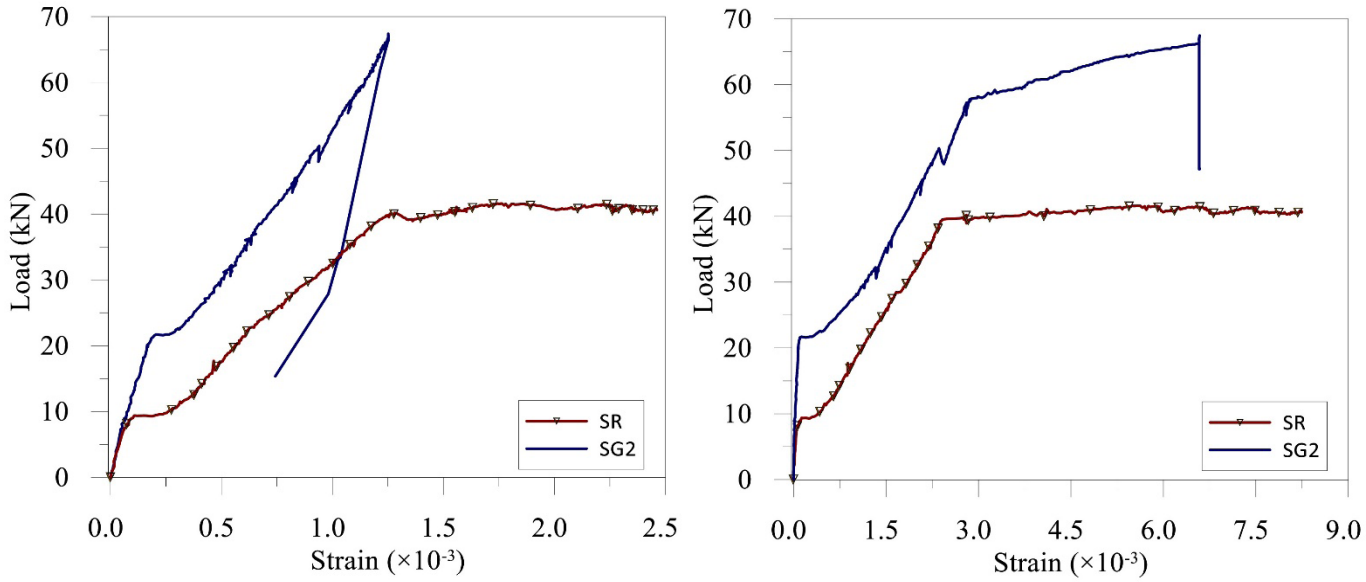

a) Load vs. Compressive strain in concrete *b) Load vs. Tensile strain in steel rebar*

Figure 7: Load–strain response of concrete and reinforcement in control and strengthened slabs

The strain responses in Figure 7 further clarify the governing material mechanisms. The steel tensile strain–load relationship indicates that SR experiences a rapid strain escalation after cracking, reflecting a higher demand on the internal steel once the tensile concrete becomes ineffective. Steel yielding can be assessed by comparing the measured strain with the yield strain approximately 0.0022. The steel strain in SR clearly exceeds this threshold at high load levels, indicating that yielding is reached before peak load and governs the subsequent ductile response. This observation is consistent with the flat post-peak branch in the load–deflection curve, where increasing deformation occurs with limited load growth.

In strengthened specimens, the steel strain develops more gradually at the same load levels, confirming that the externally bonded FRCM layer carries part of the tensile force after cracking and reduces demand on the internal reinforcement. As a result, yielding is delayed: SG1 reaches the yielding threshold at a higher load than SR, and SG2

shows the most pronounced delay. This behavior is consistent with the load–deflection curves, where the strengthened specimens maintain higher stiffness in the cracked stage and require larger load increments to produce comparable deflection increases. From a structural standpoint, this indicates improved serviceability (lower crack widths and deflections at working loads) and a more favorable redistribution of tensile stresses between steel and the external fabric.

The compressive strain at the top concrete fiber provides an additional check against code-based strain limits. In ACI 318, the commonly adopted ultimate compressive strain for concrete in flexural design is around 3‰. The measured compressive strain in SR increases steadily with load but remains below this typical limit at peak load, suggesting that SR does not fail by crushing of the compression zone. Instead, SR reaches a flexural capacity governed by steel yielding and stiffness loss, followed by stable deformation. This interpretation is supported by the absence of an abrupt post-peak drop in the SR load–deflection response. For SG2 (and to a lesser extent SG1), the compressive strain increases to higher levels at peak load because the strengthened section sustains higher bending moments; however, the compressive strain remains around, or slightly below, the 3‰ benchmark at the onset of ultimate behavior, indicating that compression failure is not the primary trigger of collapse in the strengthened slabs either. Rather, the abrupt load reduction observed in SG2 near peak load is more consistent with a tensile-side limit state, such as fabric rupture, localized peeling of the cover, or sudden debonding/rupture-related instability in the strengthened layer, which can reduce tensile capacity rapidly even if the compressive strain has not exceeded the conventional crushing threshold.

SR specimen exhibits a ductile flexural response governed by steel yielding, characterized by a stable post-yield plateau and progressive deformation. In contrast, SG1 and SG2 achieve higher ultimate loads and improved post-cracking stiffness, with delayed steel yielding due to the additional tensile contribution of the FRCM layer. However, the strengthened slabs—particularly SG2—show a sharper post-peak drop, indicating a more localized tensile-side failure associated with fabric rupture or concrete cover separation. Overall, the FRCM system effectively enhances flexural capacity and serviceability, with the two-layer configuration providing the greatest strength gain but reduced post-peak ductility compared to the control specimen.

3.2 GFRP-Reinforced Geopolymer Concrete Slabs

The structural response of the GFRP-reinforced geopolymer concrete slabs (FR, FG1, and FG2) differs fundamentally from that of the steel-reinforced series, despite identical geometry and loading configuration. Although the shear span-to-effective depth ratio was approximately a/d≈4.65, which lies within the flexure-dominated range, all GFRP-reinforced specimens exhibited shear-governed failure. This behavior is attributed to the mechanical characteristics of GFRP reinforcement and the absence of transverse shear reinforcement in the slab strips.

3.2.1 Load–deflection response

The control GFRP specimen (FR) reached an ultimate load of approximately 50 kN, which is higher than the steel control specimen SR (42.4 kN). However, the post-peak response of FR was markedly different. The load–deflection curve shows a relatively steep initial slope followed by gradual stiffness degradation after cracking (Figure 8). Unlike the steel series, no clear yielding plateau is observed. Instead, the curve terminates abruptly after peak load, indicating a brittle limit state.

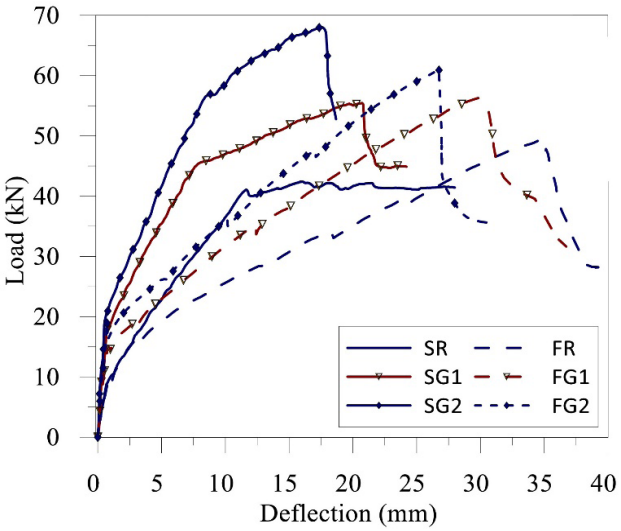

Figure 8: Effect of FRCM strengthening on load–deflection response for all specimens

For the strengthened GFRP specimens, FG1 and FG2 reached ultimate loads of approximately 56 kN (+12% relative to FR) and 60 kN (+20%), respectively. Although FRCM strengthening enhanced both stiffness and ultimate capacity, the incremental gains were moderate compared to the steel series (+31% and +59%). Moreover, the load–deflection curves of FG1 and FG2 display limited post-peak ductility and exhibit sharp load drops associated with diagonal cracking and localized failure.

At comparable midspan deflections, FG2 consistently carried higher loads than FR and FG1, confirming that the externally bonded FRCM layer contributed to tensile force redistribution. However, the strengthening effect tended to saturate: increasing from one to two fabric layers yielded only a 4 kN gain, suggesting that the governing failure mechanism was not controlled by flexural capacity alone.

3.2.2 Strain development and material limits

The absence of yielding behavior in the GFRP reinforcement plays a critical role in the observed structural response. With a modulus of elasticity of approximately 45 GPa—significantly lower than steel (200 GPa)—the tensile strain in the GFRP bars increases rapidly even at moderate load levels (Figure 9-b). Because GFRP behaves linearly elastic up to rupture, no plastic redistribution of internal forces occurs. As a result, once cracking initiates, tensile stresses concentrate more severely in both the longitudinal reinforcement and the surrounding concrete.

The compressive strain in the top fiber of FR and FG specimens remained below the ACI 318 ultimate compressive strain limit of 3‰, indicating that compression crushing was not the governing failure mechanism (Figure 9-a). According to ACI Committee 440 (2015), FRP reinforcement remains linearly elastic up to rupture and does not provide plastic redistribution capacity, which increases the susceptibility of members to brittle failure modes. Instead, failure occurred prior to reaching the conventional flexural compression limit. This confirms that the ultimate limit state was governed by shear-related mechanisms rather than by flexural compression failure.

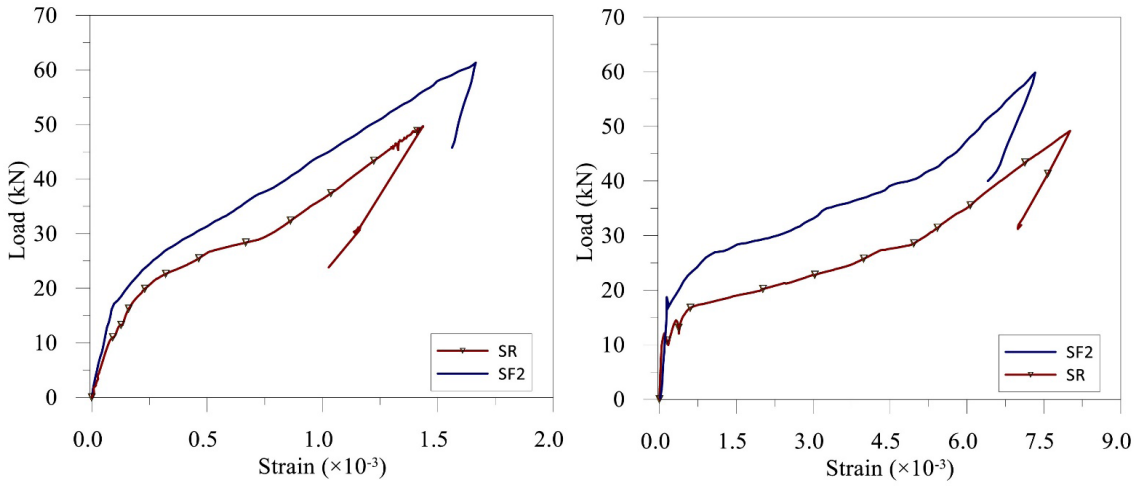

a) Load vs. Compressive strain in concrete *b) Load vs. Tensile strain in GFRP reinforcement*

Figure 9: Load–strain response of concrete and reinforcement in control (SR) and strengthened (SF2) slabs

3.2.3 Shear failure mechanism

Despite an *a/d* ratio consistent with flexural dominance, the GFRP slabs developed diagonal cracking within the shear spans. The critical explanation lies in the interaction between reduced stiffness, wider crack opening, and limited shear transfer mechanisms.

The lower modulus of GFRP leads to larger tensile strains and wider flexural cracks at service and near-ultimate loads. Increased crack width reduces aggregate interlock across crack surfaces, which is one of the primary mechanisms contributing to concrete shear resistance in members without stirrups. Additionally, dowel action of GFRP bars is less effective than that of steel due to lower stiffness and different surface characteristics. Consequently, the effective shear resistance of the cracked section decreases significantly once diagonal cracking initiates.

For FR, the applied load of 50 kN corresponds to a shear force of approximately 25 kN at each support under four-point bending. As the section cracks and flexural stiffness degrades, principal tensile stresses in the shear span increase, leading to diagonal tension cracking. Once a critical shear crack forms, the absence of stirrups prevents redistribution of shear stresses, resulting in brittle failure.

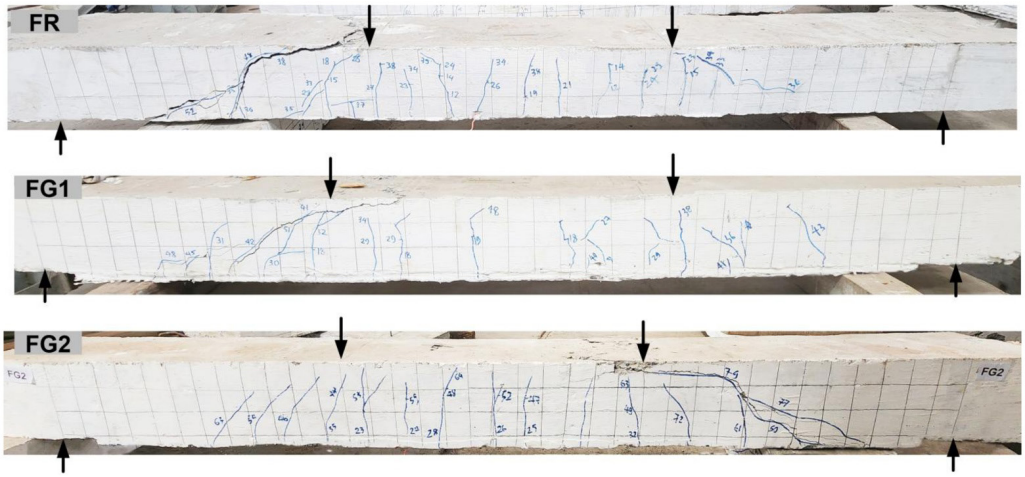

Figure 10: Crack patterns at failure of GFRP-reinforced slabs

In FG1 and FG2, the FRCM layer enhances flexural stiffness and delays crack initiation in the constant moment region. However, because the FRCM overlay was applied only at the soffit and not wrapped along the sides, its contribution to shear resistance was limited. The externally bonded fabric primarily improves tensile capacity but does not significantly increase shear capacity in the web region. As a result, while bending resistance increases moderately (to 56–60 kN), the shear capacity remains the governing limit state. The strengthening therefore shifts the stress distribution but does not eliminate the critical shear vulnerability.

This explains why the percentage increase in ultimate load is relatively modest and why the failure mode remains shear-dominated. In fact, the sharper post-peak drops observed in FG2 suggest that increasing flexural capacity without proportionally enhancing shear capacity can lead to more sudden shear failure once diagonal cracking propagates.

The crack patterns are consistent with the mechanical interpretation. In FR, diagonal cracks formed within the shear spans and propagated toward the loading points (Figure 10), with crack angles between 30° and 45°, typical of diagonal tension failure. In FG1 and FG2, flexural cracks were more uniformly distributed in the constant moment region, indicating improved crack control by the FRCM layer. However, once critical diagonal cracks developed near the supports, failure progressed rapidly. Although FG2 exhibited a denser crack network prior to collapse, the ultimate failure remained governed by diagonal cracking rather than flexural compression or bar rupture.

These observations confirm that the GFRP series is controlled by the shear capacity of the cracked geopolymer section. In contrast to the ductile flexural behavior of steel-reinforced slabs, the GFRP specimens exhibited brittle shear-dominated failure. The FRCM layer enhanced flexural performance but did not fundamentally modify the governing shear mechanism.

4 NUMERICAL ANALYSIS

4.1 Modeling techniques

Three-dimensional nonlinear finite element (FE) models were developed in ATENA to reproduce the experimental behaviour of both control and FRCM-strengthened slab strips. Owing to geometric symmetry and the symmetric four-point bending configuration, only half of the slab was modelled to improve computational efficiency while preserving solution accuracy. The model geometry, loading arrangement, and boundary conditions were defined to closely represent the laboratory setup, including the support regions and loading blocks (Figure 11). In the numerical simulations, flat rectangular support plates were used instead of the cylindrical roller supports adopted in the experiments in order to enhance numerical stability and mitigate local stress concentration, while maintaining an equivalent global structural response.

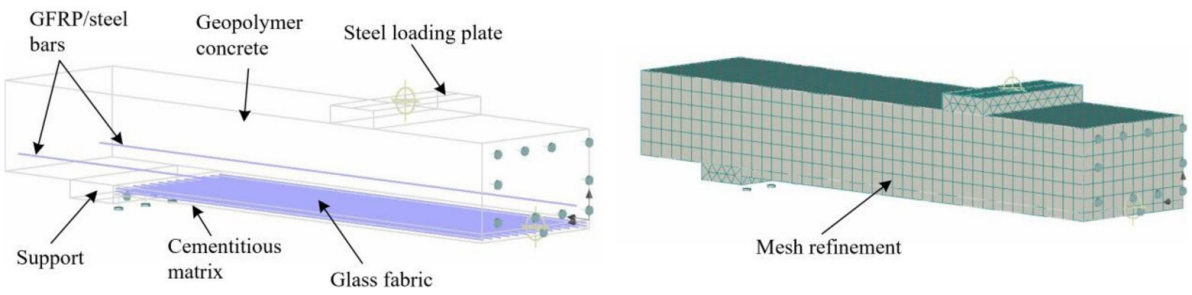

Figure 11: Numerical model and mesh refinement

The geopolymer concrete slab and the cementitious matrix of the FRCM layer were modeled using ATENA's 3D Nonlinear Cementitious 2 material model, which incorporates fracture mechanics-based cracking, tension softening, compression hardening–softening, and stiffness degradation. Material parameters were defined primarily from the experimentally measured compressive strength, tensile strength, and elastic modulus of the geopolymer concrete and mortar. This formulation allows realistic simulation of crack initiation, propagation, and crushing under flexural loading.

Longitudinal steel reinforcement was modeled using embedded truss elements with a bilinear elastic–perfectly plastic constitutive law. The elastic modulus was set to 200 GPa and the yield strength was defined according to the experimental value (439.6 MPa). For GFRP bars, a linear elastic material model was adopted up to failure, consistent with their experimentally observed behavior, with an elastic modulus of 45 GPa and tensile strength of 810 MPa. The glass fabric within the FRCM layer was modeled as embedded linear elastic reinforcement with its measured tensile properties.

To simplify the analysis and maintain consistency with the experimental observations—where no premature debonding was recorded—a perfect bond assumption was adopted between concrete and internal reinforcement, as well as between the FRCM layer and the concrete substrate. No interface elements were introduced; instead, compatibility of displacements was enforced between materials. This assumption is justified by the strong bond performance observed in pull-out and composite tensile tests, and it avoids introducing additional uncertainty associated with interface parameter calibration.

The concrete and FRCM layer were discretized using 3D solid elements with an average mesh size of approximately 25 mm, which was verified to provide stable crack patterns without excessive computational cost. Loading was applied in displacement-control through incremental vertical displacement of the loading plate, allowing stable tracing of the post-cracking and post-peak response. This approach ensured accurate capture of stiffness degradation, strain redistribution, and ultimate failure mechanisms consistent with the experimental results.

4.2 Numerical simulation results and validation

The finite element (FE) simulations demonstrate good agreement with the experimental load–deflection responses for both steel- and GFRP-reinforced slab series. Figures comparing experimental and numerical curves show that the global structural behavior, cracking-induced stiffness degradation, and ultimate capacity are reproduced with acceptable accuracy.

4.2.1 Steel-reinforced series

For the control specimen SR, the FE model accurately captures both the initial linear elastic response and the post-cracking stiffness degradation (Figure 12). The predicted ultimate load slightly overestimates the experimental value by approximately 2% (FEM/EXP = 1.02), which demonstrates very good agreement. The model reproduces the yielding-controlled behavior observed experimentally, although the numerical post-peak branch appears somewhat steeper. This difference is attributed to the assumption of perfect bond and the absence of localized slip and crack-opening mechanisms in the numerical formulation.

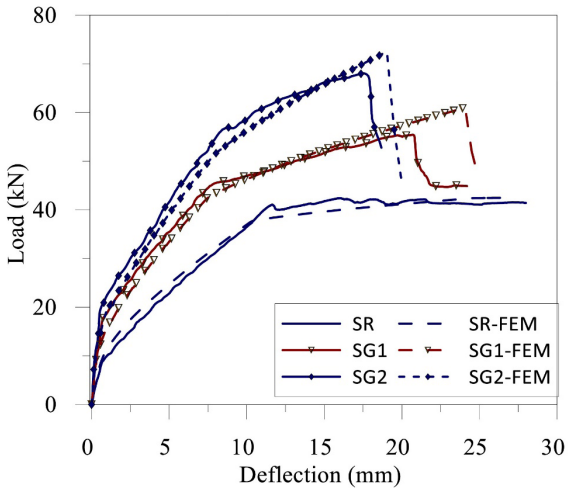

Figure 12: Comparison of experimental and FEM load–deflection responses for steel-reinforced slabs

For the strengthened specimens SG1 and SG2, the FE model also shows good predictive capability. The ultimate loads are overestimated by approximately 10% and 7%, respectively. The post-cracking stiffness enhancement provided by the FRCM layer is well reproduced, and the overall shape of the load–deflection curves matches the experimental trend. In SG2, the numerical model predicts a slightly sharper post-peak drop, reflecting localized tensile failure in the

FRCM layer and progressive compression softening in the concrete.

Stress contours at ultimate load indicate that tensile stresses are primarily carried by the steel reinforcement and the FRCM layer, while compressive stresses in the top concrete fiber remain below the compressive capacity of the geopolymer concrete. The simulated steel strain exceeds the yield strain (≈2.2‰), confirming that the steel has yielded prior to failure. Final failure is governed by rupture of the glass fabric in the constant moment region, with predominantly vertical flexural cracks, consistent with the experimental observations.

4.2.2 GFRP-reinforced series

For the GFRP control specimen FR, the FE model predicts the ultimate load with a deviation of approximately 13% (FEM/EXP = 1.13), which is noticeably larger than the discrepancy observed in the steel-reinforced specimen (≈2%). Although the overall load–deflection trend is reasonably captured, the difference in peak load indicates a reduced predictive accuracy for the GFRP system compared to the steel series. The numerical response correctly reproduces the absence of a yielding plateau and the abrupt post-peak drop associated with the brittle behavior of GFRP-reinforced members (Figure 13). Concrete compressive strain remains below the crushing limit at peak load, confirming that failure is not governed by concrete compression. Stress contours show high tensile stresses in the GFRP bars, while principal tensile stresses concentrate within the shear spans of the concrete. The inclined stress trajectories (approximately 35–45°) correspond closely to the experimentally observed diagonal crack patterns, indicating shear-dominated behavior rather than flexural rupture of the GFRP bars.

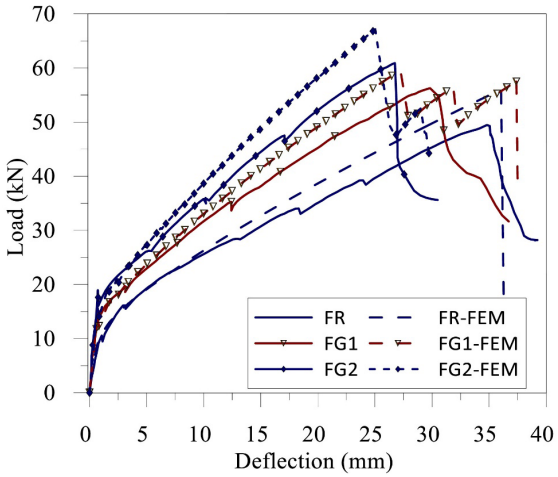

Figure 13: Model validation: experimental versus FEM load–deflection response of GFRP-reinforced slabs

For the strengthened specimens FG1 and FG2, the FE model overestimates the ultimate load by approximately 6% and 10%, respectively. Although the agreement is acceptable, the deviations remain consistently higher than those observed in the steel-reinforced series. This suggests that the numerical model captures flexure-controlled behavior more accurately than shear-controlled mechanisms. Crack pattern visualization confirms that diagonal cracks initiate within the shear spans and propagate rapidly once the principal tensile stress exceeds the tensile strength of the geopolymer concrete. In FG2, the increased flexural stiffness elevates shear demand, accelerating the formation of the critical inclined crack. Consequently, failure remains shear-controlled despite the additional strengthening layer.

4.2.3 Stress distribution and crack propagation

The stress distribution contours provide further insight into the governing failure mechanisms. In the steel-reinforced configuration (SG2-FEM, Figure 14-a), failure is governed by flexural cracking characterized by predominantly vertical cracks in the constant moment region. The final failure occurs due to rupture of the glass fabric at midspan. At this stage, the internal steel reinforcement has already yielded, indicating full development of flexural capacity. Once fabric rupture takes place, the tensile stress in the textile layer at the crack location drops abruptly to nearly zero due to stress release. Meanwhile, the compressive stresses in the geopolymer concrete remain significantly lower than its compressive strength, confirming that failure is not controlled by concrete crushing but by tensile rupture of the strengthening layer.

In contrast, for the GFRP-strengthened model (FG2-FEM, Figure 14-b), failure is governed by an inclined crack developing within the shear span, indicating shear-controlled behavior. The dominant diagonal crack forms after the development of flexural cracks and rapidly propagates toward the loading point, triggering failure. Unlike the steel-

reinforced case, both the glass textile and the internal GFRP bars remain within the elastic range at ultimate load, without reaching rupture or yielding. This suggests that the available flexural capacity is not fully mobilized. Instead, the increased flexural stiffness and strength provided by the GFRP reinforcement elevate the shear demand in the critical regions. As the shear resistance is not proportionally enhanced, diagonal tension failure governs the response. The stress contours further show concentrated principal tensile stresses along the inclined crack path, consistent with the experimentally observed shear failure mechanism.

Overall, the FE model predicts the ultimate loads of the steel-reinforced slabs with deviations ranging from approximately 2% to 10%, while slightly larger discrepancies of about 6% to 13% are observed for the GFRP-reinforced slabs. Despite this difference in accuracy, the model successfully captures the transition in governing failure mode—from flexure-controlled behavior in the steel series to shear-controlled behavior in the GFRP series. The slightly higher numerical stiffness is mainly attributed to the assumptions of perfect bond and material homogeneity adopted in the finite element formulation.

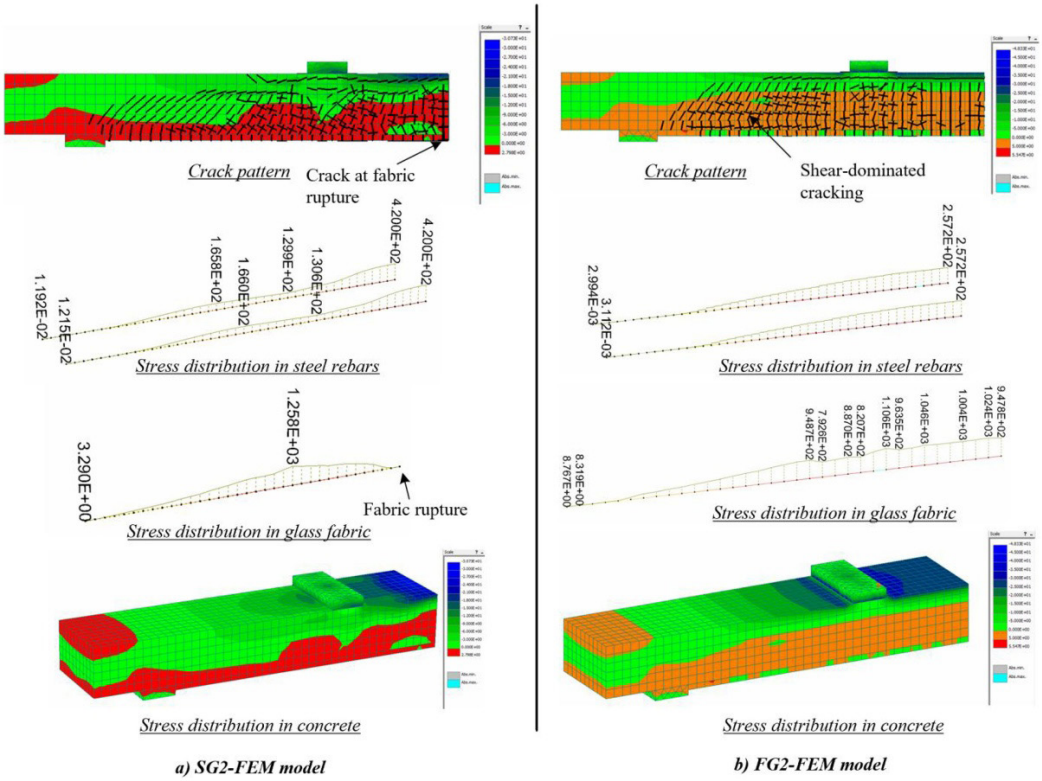

Figure 14: Comparison of failure mechanisms and stress distributions obtained from FEM analysis

5 CONCLUSIONS

This study provides an integrated experimental–numerical assessment of glass TRC strengthening applied to geopolymer concrete (GPC) slabs reinforced with either steel or GFRP bars. The work clarifies how internal reinforcement type governs the structural response and strengthening efficiency.

For steel-reinforced GPC slabs, TRC strengthening enhanced ultimate capacity by approximately 31% and 59% for one and two layers, respectively, while preserving flexure-controlled failure. The results confirm that TRC effectively increases tensile force capacity and crack-bridging action without compromising ductility when yielding reinforcement is present.

For GFRP-reinforced slabs, the corresponding strength gains were more moderate (13.7-23.1%), and failure remained shear-dominated. The absence of yielding and the lower stiffness of GFRP led to higher tensile strains and earlier diagonal crack development, limiting the effective utilization of the enhanced flexural capacity. This highlights a fundamental shift in governing mechanism when replacing steel with GFRP in geopolymer members.

The validated FE model predicted the ultimate loads with deviations of about 2–10% for the steel-reinforced slabs and 6–13% for the GFRP-reinforced slabs. It successfully reproduced the shift from flexure-controlled to shear-dominated failure, capturing the load–deflection response and crack development with satisfactory accuracy.

The results indicate that glass-FRCM strengthening enhances the flexural capacity of steel-reinforced GPC slabs;

however, it appears insufficient to prevent shear-dominated responses in GFRP-reinforced systems, suggesting the necessity of integrated flexural–shear strengthening strategies. Owing to the relatively limited number of specimens and the absence of repeated tests, the present findings should be interpreted as indicative rather than statistically conclusive, and further investigations involving larger experimental datasets are therefore recommended.

Acknowledgments

This research is funded by University of Transport and Communications (UTC) under grant number T2024-XD-002TD.

Author's Contributions: Conceptualization, HC Nguyen and TC Dang; Methodology, HC Nguyen; Investigation, TC Dang and CH Nguyen; Formal analysis, TC Dang; Writing – original draft, TC Dang; Writing – review & editing, HC Nguyen; Supervision, HC Nguyen; Resources, HC Nguyen; Funding acquisition, TC Dang.

Data Availability: Research data is only available upon request

Editor: Marcílio Alves

References

Udhaya Kumar, T., Vinod Kumar, M., Lakkaboyana, S.K., Trilaksana, H., Ansari, A. (2025). Investigation of bond strength and flexural behaviour of geopolymer aggregate concrete beams. Case Studies in Construction Materials 22: e04916.

Kadhim, A.J., Zinkaah, O.H. (2025). Numerical and theoretical investigation for the flexural behaviour of geopolymer concrete beams reinforced with hybrid FRP/steel bars. Journal of Building Engineering 101: 111883.

Hasan, M.A., Sheehan, T., Ashour, A., Elkezza, O. (2023). Flexural behaviour of geopolymer concrete T-beams reinforced with GFRP bars. Structures 49: 345–364.

Junaid, M.T., Elbana, A., Altoubat, S. (2020). Flexural response of geopolymer and fiber reinforced geopolymer concrete beams reinforced with GFRP bars and strengthened using CFRP sheets. Structures 24: 666–677.

Maranan, G.B., Manalo, A.C., Benmokrane, B., Karunasena, W., Mendis, P. (2015). Evaluation of the flexural strength and serviceability of geopolymer concrete beams reinforced with glass-fibre-reinforced polymer (GFRP) bars. Engineering Structures 101: 529–541.

Azunna, S.U., Aziz, F.N.A.A., Rashid, R.S.M. (2025). Review on structural characteristics of reinforced geopolymer concrete. Progress in Engineering Science 2: 100083.

George, G., Shreeram, P.K., Minalan, A.S., Lokesh, K., Mano, M., Prince, A. (2023). Numerical investigation on the flexural behavior of geopolymer concrete beam reinforced with different types of fiber-reinforced polymer bars. Materials Today: Proceedings.

A V, N., S, D.R., Soman, M. (2025). Flexural behaviour of ternary blended ambient cured geopolymer concrete slabs. Procedia Structural Integrity 70: 215–222.

Zhang, H.Y., Liu, H.Y., Kodur, V., Li, M.Y., Zhou, Y. (2022). Flexural behavior of concrete slabs strengthened with textile reinforced geopolymer mortar. Composite Structures 284: 115220.

Alexander, A.E., Shashikala, A.P. (2024). Behavior of RC beams rehabilitated using carbon textile reinforced geopolymer mortar in flexure. Structures 69: 107522.

Elsamak, G., Ghalla, M., El-Naqeeb, M.H., Iskander, Y., Bazuhair, R.W., Yehia, S.A. (2025). Assessment of FRCM jacket configurations for enhancing shear strength of deficient RC beams. Structures 80: 109846.

Soliman, O.E., Refai, A.E., Sorelli, L. (2025). Shear strengthening of RC beams with fabric-reinforced cementitious matrix: Analytical modeling and machine learning approaches. Composite Structures 373: 119595.

Kadhim, M.M.A., Jawdhari, A., Adheem, A.H., Fam, A. (2022). Analysis and design of two-way slabs strengthened in flexure with FRCM. Engineering Structures 256: 113983.

Scheerer, S., Zobel, R., Müller, E., Senckpiel-Peters, T., Schmidt, A., Curbach, M. (2019). Flexural strengthening of RC structures with TRC—Experimental observations, design approach and application. Applied Sciences 9: 1322.

D'Ambrisi, A., Focacci, F. (2011). Flexural strengthening of RC beams with cement-based composites. Journal of Composites for Construction 15: 707–720.

Schladitz, F., Frenzel, M., Ehlig, D., Curbach, M. (2012). Bending load capacity of reinforced concrete slabs strengthened with textile reinforced concrete. Engineering Structures 40: 317–326.

ACI COMMITTEE 440 (2015). Guide for the Design and Construction of Structural Concrete Reinforced with FRP Bars (ACI

440.1R-15). American Concrete Institute, Farmington Hills, MI, USA.

ACI COMMITTEE 549 (2020). Guide to Design and Construction of Externally Bonded Fabric-Reinforced Cementitious Matrix (FRCM) Systems for Repair and Strengthening Concrete and Masonry Structures (ACI 549.4R-20). American Concrete Institute, Farmington Hills, MI, USA.